ARTIFICIAL INTELLIGENCE (AI) ANALYSIS OF HISTOLOGICAL IMAGES ACCURATELY IDENTIFIES LUMINAL SUBTYPE UROTHELIAL CARCINOMAS CHARACTERIZED BY HIGH PEROXISOME PROLIFERATOR-ACTIVATED RECEPTOR GAMMA (PPARG) EXPRESSION

Abstract: 35011

Stefan Kirov[1*], Chintan Parmar[2*], William W. Motley[1], Bijal C. Kakrecha[1], Michael G. Drage[2‡], Ben Glass[2], Ruby Hsu[2‡], Jacqueline Brosnan-Cashman[2], Ilan Wapinski[2‡], Michael Montalto[2], Andrew H. Beck[2], Matthew Bronnimann[2^], Michaela Bowden[1^]

[1]Flare Therapeutics, Cambridge, Massachusetts; [2]PathAI, Boston, Massachusetts

*Co-primary author; ^Co-corresponding author; ‡Employee of PathAI at the time this study was performed

BACKGROUND

- Muscle-invasive urothelial carcinoma (MIUC) can be broadly classified into luminal and non-luminal subtypes.
- As FX-909[1], a PPARG inverse agonist, enters the clinic, biomarkers that reflect the luminal subtype are likely to reveal patients with the potential to respond to PPARG inhibition[2].
- The determination of luminal status is generally performed via RNA-seq and/or multiple immunohistochemistry stains, which are costly and time-consuming[1].
- The luminal lineage subtype accounts for ~65% of all advanced UC[3] and is associated with the transcription factor peroxisome proliferator-activated receptor gamma (PPARG).
- MIUC tumor specimens are routinely stained with hematoxylin and eosin (H&E). AI-driven analyses of H&E-stained tissue may enable the identification of patients with luminal (PPARG-dependent) MIUC, with potential to respond to a PPARG-targeting therapy.

METHODS

- H&E-stained slides from 367 unique primary MIUC cases from the TCGA BLCA dataset were split into training (70%), validation (15%), and held-out test (15%) sets by preserving the data distribution of patient metadata.
- A retrospective cohort of 42 localized, stage III-IV MIUC, was used as an independent test set.
- Molecular classification as non-luminal (basal-squamous and neuronal subtypes) or luminal (luminal, luminal papillary, and luminal infiltrated subtypes) was performed using non-negative matrix factorization (NMF) rank 5 following the Robertson method[1].
- Pretrained artifact and tissue segmentation models were deployed on all images to identify artifact-free areas of cancer and cancer-associated stroma.
- An end-to-end (E2E) additive multiple-instance learning (MIL) model[4] was trained to identify luminal cases using the training set.

FIGURE 1. Additive MIL Schematic

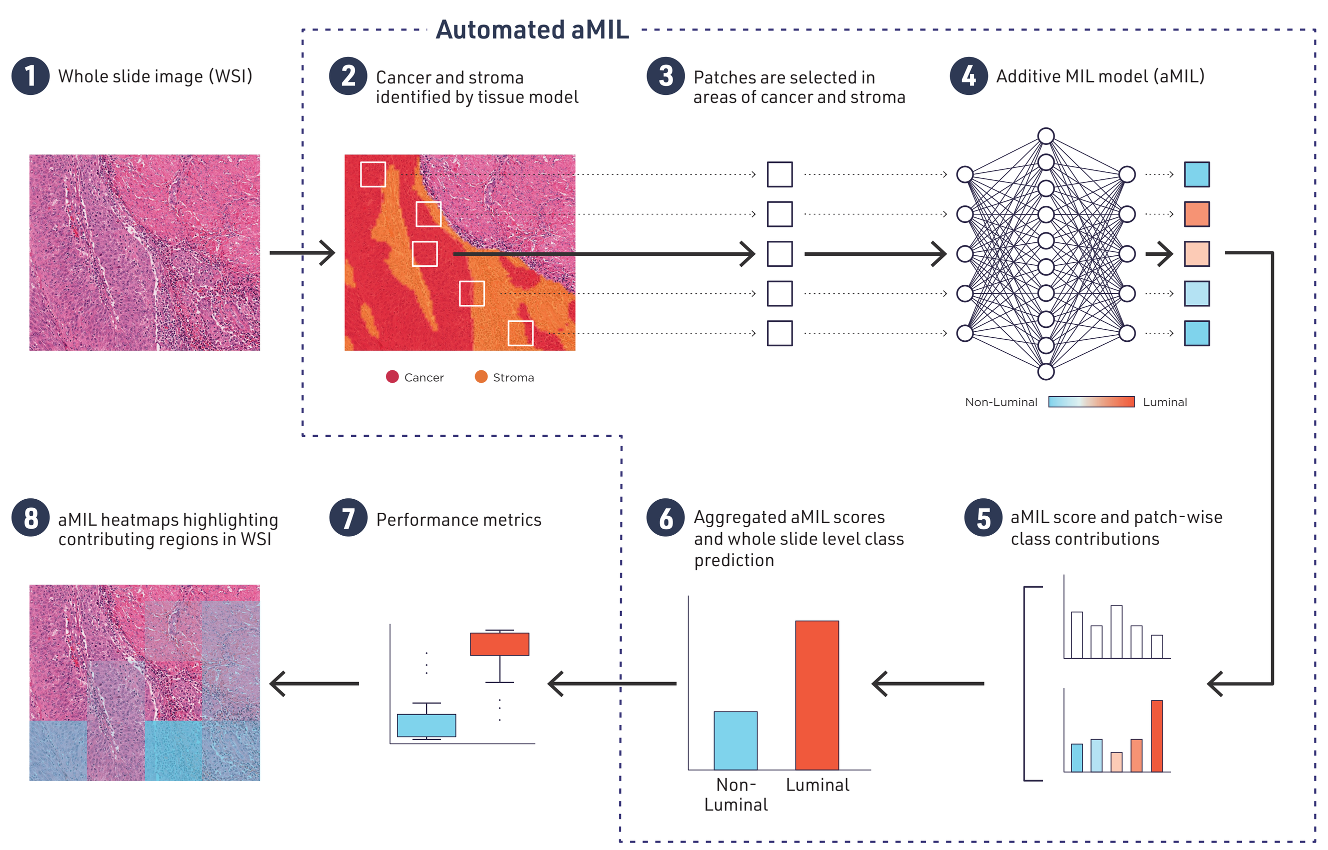

Automated aMIL
1 Whole slide image (WSI)
2 Cancer and stroma identified by tissue model
3 Patches are selected in areas of cancer and stroma
4 Additive MIL model (aMIL)
Cancer
Stroma
Non-Luminal
Luminal
5 aMIL score and patch-wise class contributions
6 Aggregated aMIL scores and whole slide level class prediction
Non-Luminal
Luminal
7 Performance metrics
8 aMIL heatmaps highlighting contributing regions in WSI

TABLE 1. Cohort Metadata and Subtype

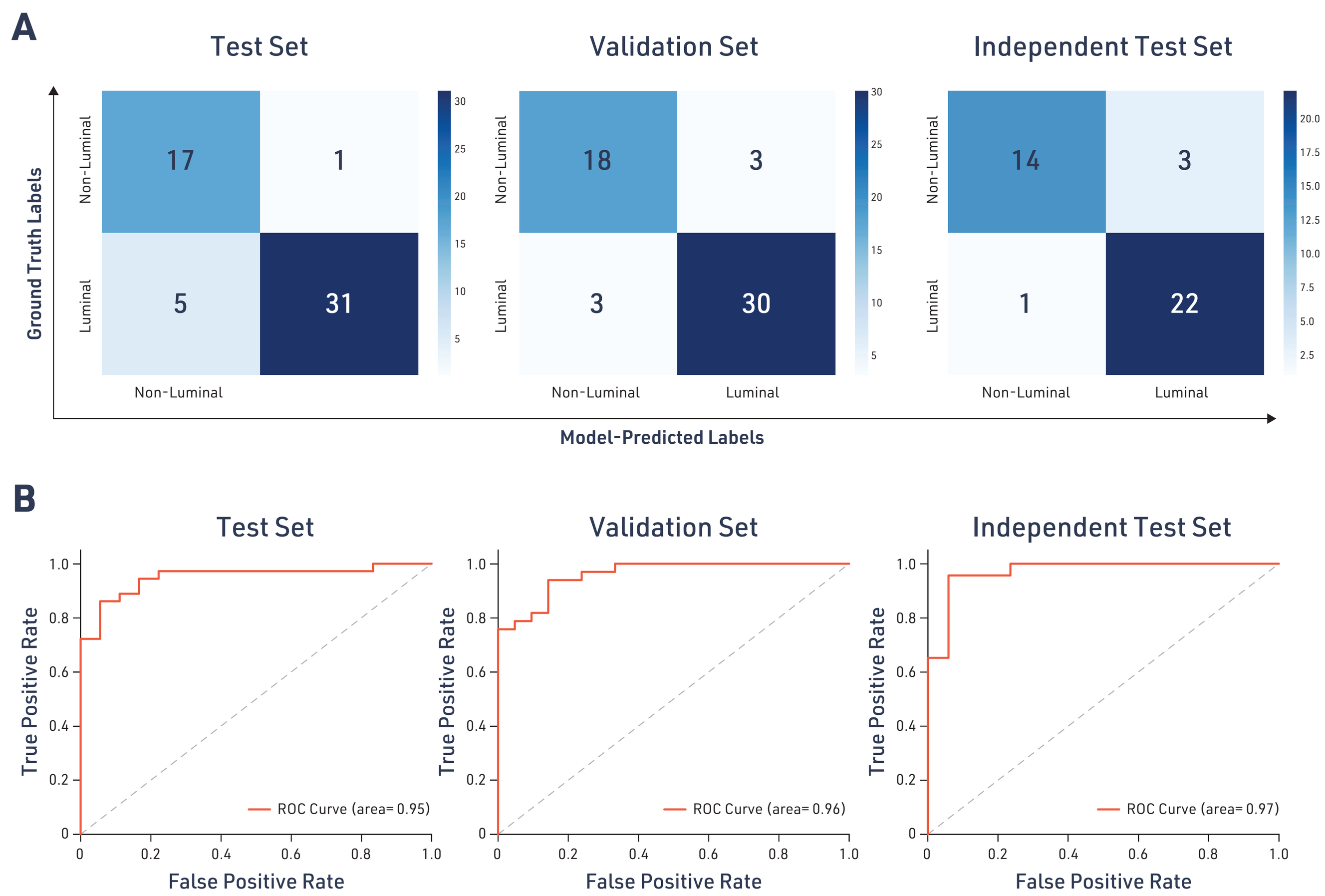
	TCGA Dataset Training Set (N=260)	TCGA Dataset Validation Set (N=54)	TCGA Dataset Test Set (N=56)	Independent Test Set (N=40)
Age				
Median	68	68.5	73	71
Range	[34 - 90]	[42 - 90]	[48 - 90]	[49 - 88]
Gender				
Male	192	45	38	26
Female	68	9	18	14
Smoking History				
Never Smoker	70	13	14	7
Former Smoker	122	28	30	9
Current Smoker	61	12	10	3
ND	7	1	2	21
Histologic Grade				
T1	244	50	54	–
T2	15	4	1	6
T3	1	–	1	24
T4	–	–	–	10
Robertson[3] Molecular Subtype				
Basal-Squamous	92	20	17	14
Neuronal	14	1	1	3
Luminal-Infiltrated	47	15	9	15
Luminal-Papillary	88	19	21	7
Luminal	17	1	7	1
ND	2	–	1	–

ND – Not determined; **Age** – Age at diagnosis for TCGA data, age at specimen collection for independent test set.

RESULTS

We assessed the ability of the E2E model to predict for luminal subtype, revealing excellent performance in the TCGA validation, TCGA test, and independent test sets.

FIGURE 2. Performance of the model in predicting luminal from non-luminal MIUC

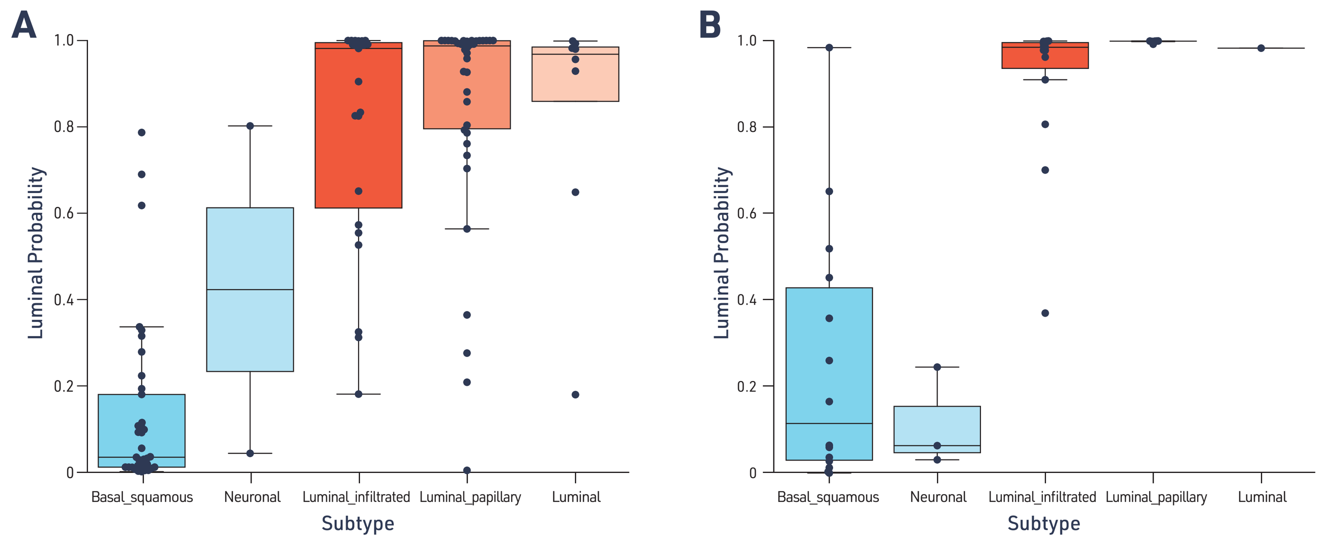

A
Test Set
Validation Set
Independent Test Set
Ground Truth Labels
Non-Luminal
Luminal
17
1
5
31
18
3
3
30
14
3
1
22
Model-Predicted Labels
B
Test Set
Validation Set
Independent Test Set
True Positive Rate
False Positive Rate
ROC Curve (area= 0.95)
ROC Curve (area= 0.96)
ROC Curve (area= 0.97)

A. Confusion matrices comparing model-predicted labels with ground truth labels derived from the molecular signatures described in Robertson et al. **B.** ROC curves depicting accuracy of model in predicting luminal status of MIUC cases.

TABLE 2. Performance of E2E model in predicting luminal MIUC. A probability of 0.5 was used as a cut-point

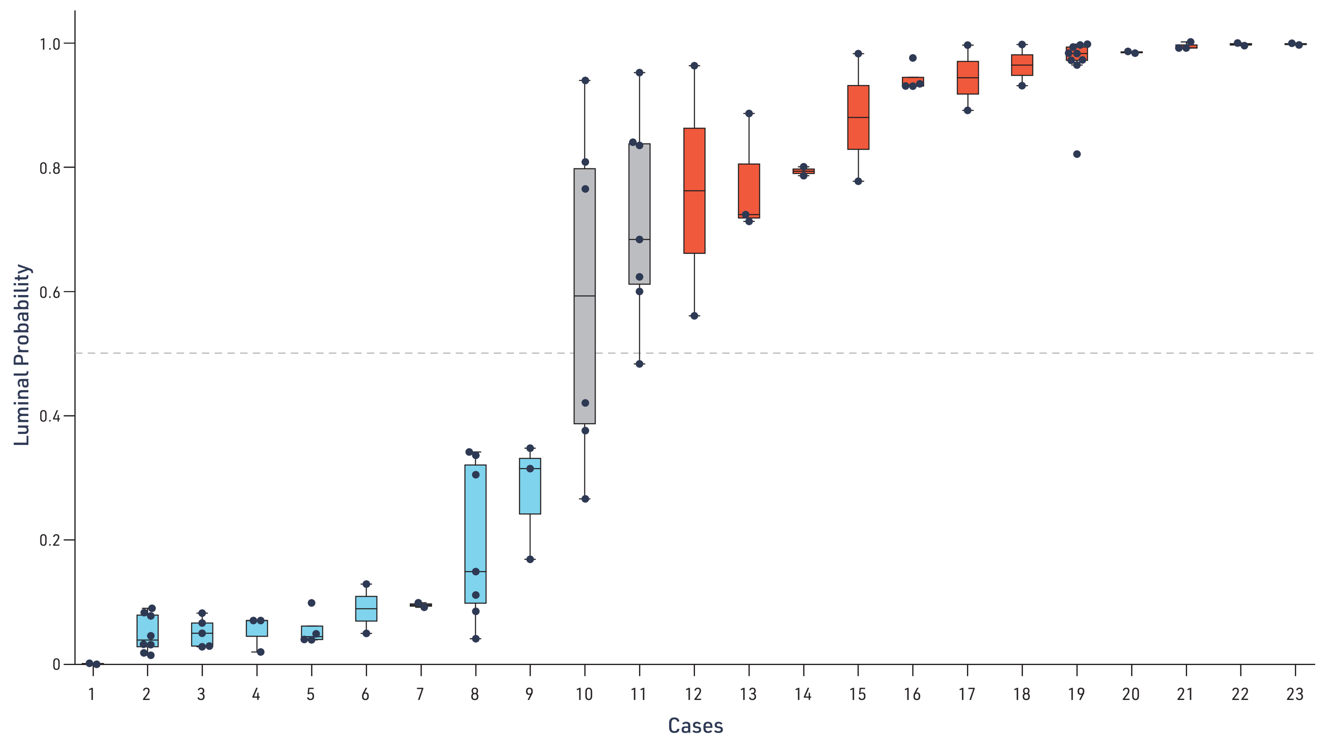
Dataset	AUC	Accuracy	Sensitivity	Specificity	Cohen's Kappa
TCGA Validation	0.96	0.89	0.91	0.86	0.77
TCGA Test	0.95	0.89	0.86	0.94	0.76
Independent Test	0.97	0.9	0.96	0.82	0.79

FIGURE 3. Model subtype prediction mirrors findings from transcriptomic analysis


A
B
Luminal Probability
Basal_squamous
Neuronal
Luminal_infiltrated
Luminal_papillary
Luminal
Subtype

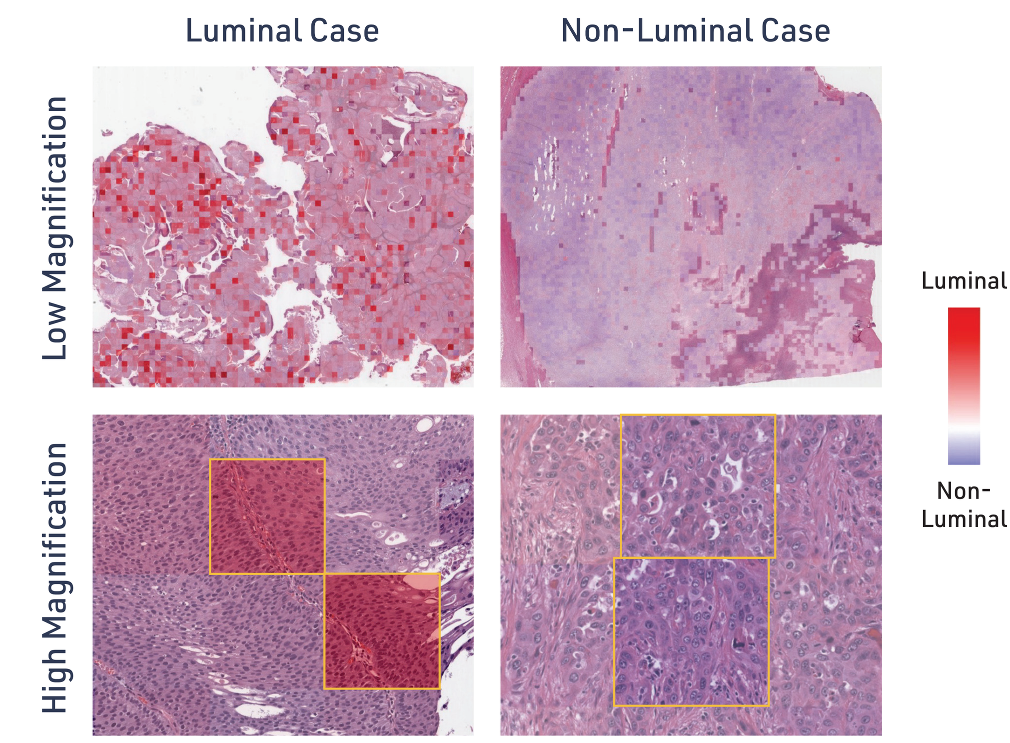
Consistent with observations from the transcriptomic scoring, luminal probability scores showed a trend within the Robertson molecular subtypes[1] increasing from luminal infiltrated, to luminal papillary, and to luminal. These observations were consistent in a combined TCGA validation and test set (**A**) and in the independent test set (**B**).

FIGURE 4. Consistency of model-predicted luminal status across multiple slides from the same case


Luminal Probability
Cases

In the initial model development only 1 replicate was used per case. After the model was developed, intra-case and inter-sample consistency was investigated. Cases with a probability greater than 0.5 (red line) were predicted to be luminal. Each box plot shows the distribution of scoring across replicates for each case. Only 2 out of 23 cases assessed had specimens with inconsistent luminal/non-luminal scoring. 80/84 replicates consistently determined luminal status. Basal cancer in cyan, luminal in red and undetermined in grey.

FIGURE 5. Areas driving prediction of luminal status in images of H&E-stained tissues can be interpreted by pathologists to generate hypotheses


Luminal Case
Non-Luminal Case
Low Magnification
High Magnification
Luminal
Non-Luminal

Patches generated by the E2E model can be converted into attention heatmaps that show how each patch is interpreted by the model. Example images of the attention heatmaps are shown. Qualitative review by a pathologist of heatmaps identified possible associations between luminal status and observable histological features, specifically areas of expansile cancer growth with minimal stroma, lacking single cell necrosis. Non-Luminal status was associated with an infiltrative growth pattern and more admixed cancer/stroma, more inflammation, and the presence of pseudoglandular configuration and single cell necrosis. These observations are useful for hypothesis generation for further exploration.

CONCLUSIONS

- High PPARG expression is a defining feature of luminal MIUC in the advanced and metastatic setting[3].
- We generated a robust AI-based model that accurately predicts luminal MIUC using H&E-stained slides.
- The independent test set is a cohort of patients with higher grade UC, who are more likely to progress to the advanced and metastatic setting where the activity of FX-909 will be tested in early phase clinical trials. In this collection of higher grade cases, the algorithms performance was similarly accurate and a similar proportion of patients had a luminal subtype.
- The strong performance of the model highlights the potential for its application as a precision biomarker to identify patients with advanced UC that may respond to PPARG inhibition.
- FX-909, a PPARG inverse agonist, entering the clinic represents a promising potential therapy for patients with advanced UC harboring the luminal subtype.

References

1. Robertson AG, et al. *Cell*. 2017 171(3): 540-556.e25.
2. Sims R, "New Drugs on the Horizon: Part 2", 16th April, AACR, Orlando, Fl.
3. Motley, W, et al. *Eur J Cancer*. 2022 174(S1): S119.
4. Javed, SA, et al. *Adv Neural Inf Process Syst*. 2022 35: 20689-702.

www.flaretx.com/publications

Scan to View Poster Abstract #35011